ELSEVIER

Chemical Engineering Journal 109 (2005) 115–122

Chemical Engineering Journal

www.elsevier.com/locate/cej

# Multiphase flow characteristics of a novel internal-loop airlift reactor

Tongwang Zhang, Jinfu Wang *, Zi Luo, Yong Jin

*Department of Chemical Engineering, Tsinghua University, Beijing 100084, PR China*

Received 31 August 2004; received in revised form 24 March 2005; accepted 30 March 2005

**Abstract**

One important challenge in chemical industry, especially for processes of synthesis fuels, is the development of effective three-phase reactors for high pressure and temperature. In the present study, a novel airlift internal-loop reactor (ALR) was proposed and its hydrodynamic behaviors were experimentally studied. The local bubble rise velocity and liquid velocity are measured under different operating conditions. The influence of operating conditions including the superficial gas velocity and solid holdup on the bubble rise velocity and liquid velocity in the riser was studied. A mathematical model was proposed based on the energy balance to describe the multiphase flow characteristics in the internal-loop airlift reactor. The comparison between the calculated and experimental values shows that the proposed model can predict the flow behavior reasonably.


*Keywords:* ALR; Bubble rise velocity; Liquid velocity; Energy balance

## 1. Introduction

Internal-loop airlift reactors (ALR) are widely used in chemical industry and biotechnological processes, e.g. oxidation, chlorination and fermentation processes [1,2]. It is usually constructed by mounting a draught tube in a bubble column. The gas is dispersed into the draught tube or into the annulus and a global liquid circulation flow is formed. The circulating liquid flow enhances heat and mass transfer and makes the flow behavior more homogeneous in the reactor [3]. In the three-phase system with suspended solids, the particles can be completely suspended at lower gas velocity in an ALR compared with a bubble column [4].

The gas–liquid separator at the top of the reactor has important influence on the performance of the ALRs [5,6]. This influence is a combination of its ability to separate gas from the liquid or liquid–solid phase and its hydraulic resistance. Choi et al. [6] found that in the case of a significantly restricted liquid flow area, the pressure drop through the separator was dominant over the gas separation ability. For some reactions in a three-phase system, such as the synthesis of dimethyl ether [7], the reactant and the product are gas, the liquid phase is inert solvent and the solid phase is catalyst. Bubble entrainment into the down-comer is disadvantageous to the production efficiency. Therefore, we reported in this work a novel internal-loop airlift reactor with a specially designed gas–liquid separator. This gas–liquid separator can separate gas and liquid completely even at a high gas velocity.

The multiphase flow behaviors of this novel reactor, such as the local bubble rise velocity and liquid velocity, are experimentally measured using a conductivity probe and the laser doppler velocimetry (LDV), respectively. For the purpose of design and scale-up of the reactor, a mathematical model was established based on the energy balance. The validation of the proposed mathematical model has been tested by the experimental measurements.

## 2. Experimental

The ALR used in this work is schematically shown in Fig. 1. It is made of Plexieglas and consists of two concentric tubes and an expansion as enlarged degassing zone, 820 mm in diameter. The main column is 5.6 m in height and 376 mm in inner diameter. A draft tube of 220 mm in diameter, 7 mm in thickness and 5 m in height is mounted in the column 7 cm

* Corresponding author. Tel.: +86 10 62785464; fax: +86 10 62772051.
*E-mail address:* wangjf@flotu.org (J. Wang).

1385-8947/$ – see front matter © 2005 Elsevier B.V. All rights reserved.
doi:10.1016/j.cej.2005.03.014

**Nomenclature**

| | |
|---|---|
| $A$ | cross-sectional area ($m^2$) |
| $d$ | diameter (m) |
| $E$ | energy inputted (W) |
| $f$ | friction loss (W) |
| $F$ | friction losses between liquid and device (W) |
| $g$ | gravity acceleration ($m/s^2$) |
| $H$ | vertical height (m) |
| $P$ | pressure (Pa) |
| $S$ | friction losses at the liquid–gas interface (W) |
| $u$ | local velocity (m/s) |
| $U$ | superficial velocity (m/s) |
| $W$ | friction losses due to internal recirculation (W) |

*Greek letters*

| | |
|---|---|
| $\alpha$ | coefficient |
| $\beta$ | coefficient |
| $\varepsilon$ | phase holdup |
| $\lambda$ | friction coefficient |
| $\mu$ | viscosity (Pa s) |
| $\rho$ | density ($kg\,m^{-3}$) |

*Subscripts*

| | |
|---|---|
| b | bubble |
| d | down-comer |
| g | gas phase |
| h | pseudo-homogeneous phase |
| l | liquid phase |
| r | riser |
| s | solid phase |
| t | separator tube |
| u | U-bending flow |

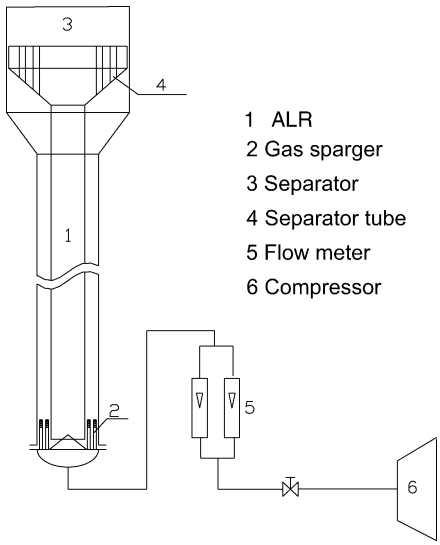


Fig. 1. Experimental set-up.

above the gas distributor. The draft tube and the annular channel between the two concentric tubes are used as the down-comer and riser, respectively.

The gas liquid separator is similar to a funnel. Its bottom is connected to the top of the draft tube and its top is equal to the expansion in diameter, as shown in Fig. 1. Twenty tubes, 35 mm in diameter, is distributed on two concentric loops and mounted at the flank of the funnel. Twelve tubes are mounted at the outer loop and 8 tubes at the inner loop uniformly. Because of the presence of the separator tubes, the abrupt constriction of flow channel makes the gas–liquid mixture eject from the tubes and improve the separation efficiency. During the experiment, there is no bubble observed being entrained into the down-comer even at high superficial gas velocity. Higher heat transfer can be obtained if the reaction takes place in the annular. So the gas is dispersed into the annulus through a special designed sparger. The sparger composed of a base plate with 20 holes onside, 20 stainless steel tubes and 20 sintered steel tubes. The 20 holes are distributed on two concentric loop at the base plate, 12 at the outer loop and 8 at the inner loop. Each sintered steel tube is connected with one stainless tube and the other end of the stainless tube is connected with the hole on the base plate. The sintered steel tube is high than the bottom of the draught tube. This can guarantee bubbles be sparged into the annulus directly. Even though there is lots of solid in the annular, bubbles would not enter the draught tube and make the liquid rises in the draught.

Air, tap water and glass beads with density of 2400 $kg/m^3$ and mean diameter of 100 μm were used as the gas, liquid and solid phase, respectively. Different solid loadings were used to investigate the influence of the solid phase on the flow behavior. The level of water or liquid–solid slurry filled in the reactor was controlled at a height of 10 cm above the top of the separator tubes. The air was fed into the annulus through the gas distributor presented previously and the flux was controlled by a calibrated rotameter. The superficial gas velocities, $U_g$, varied from 0.0076 to 0.213 m/s according to industrial applications.

The local liquid velocity in the riser was measured by a backward scattering LDA system (system 9100-8, model TSI). The measuring method and data processing were described elsewhere [8]. A conductivity probe was used to measure the bubble size and bubble rise velocity in the riser. The probe has two tips that correspond to different response time for a same bubble boundary. Therefore, bubble rise velocity can be obtained from the different response time and the distance between the two probe tips [9].

## 3. Results and discussion

### 3.1. Bubble rise velocity

It is important to study the bubble rise velocity and its radial profile in a gas–liquid system as these are closely related

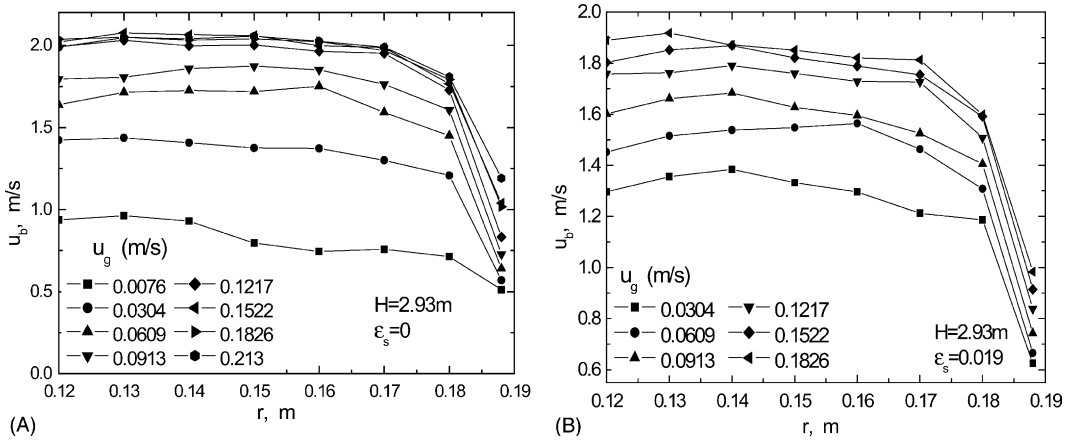


Fig. 2. The radial profile of bubble rise velocity at different superficial gas velocities.

to the hydrodynamics, mass and heat transfer [10]. Fig. 2(A) and (B) shows the radial profiles of bubble rise velocity at different superficial gas velocities with solid volume fraction of $\varepsilon_s = 0$ and $\varepsilon_s = 1.94$, respectively. Note that in the figures the $x$ coordinates 0.11 m and 0.188 m correspond to the inner and outer flow boundaries of the riser, respectively. The bubble rise velocity increases with increasing superficial gas velocity, but the increase tendency becomes weaker at high superficial gas velocities. When the superficial gas velocity exceeds 0.1217 m/s at $\varepsilon_s = 0$, the superficial gas velocity almost has no influence on the bubble rise velocity, showing that the bubble rise velocity does not increase unlimitedly with increasing superficial gas velocity and reaches a constant with increasing superficial gas velocity. For the case of $\varepsilon_s = 1.94\%$, the bubble rise velocity is smaller than that in a gas–liquid system at the same superficial gas velocity. Similarly, the increase of the bubble rise velocity at high superficial gas velocities is less than that at low superficial gas velocities. The solid particles increase the flow resistance of the system, which in turn results in a decrease in the liquid velocity.

Fig. 3 illustrates the axial evolution of the radial profile of the bubble rise velocity at $U_g = 0.1217$ m/s and $\varepsilon_s = 0$. The bubble rise velocities increase slightly with increasing axial height. Along the riser height, the bubble size becomes larger due to coalescence and pressure decrease, which in turn leads to an increase in the bubble rise velocity. At the axial position of $H = 4.23$ m, the bubble rise velocity is smaller near the wall of the draught tube than those at other axial positions.

The influence of the solid holdup at $U_g = 0.0304$ m/s on the radial profile of bubble rise velocity is shown in Fig. 4. The bubble rise velocity decreases with increasing solid holdup. With an exception, the radial profile of the bubble rise velocity remains almost unchanged as the solid holdup varies from 0.19 to 0.39%. Addition of solids has three different influences on the flow behavior, namely, accelerating the breaking rate, accelerating the coalesce rate and increasing the flow resistance [11,12]. Under different solid holdups, the dominant effect of the addition of solids is different, leading to a different influence on the bubble rise velocity.

The solid holdup also affects the radial profile of bubble rise velocity. At low solid holdups, the radial profiled of the

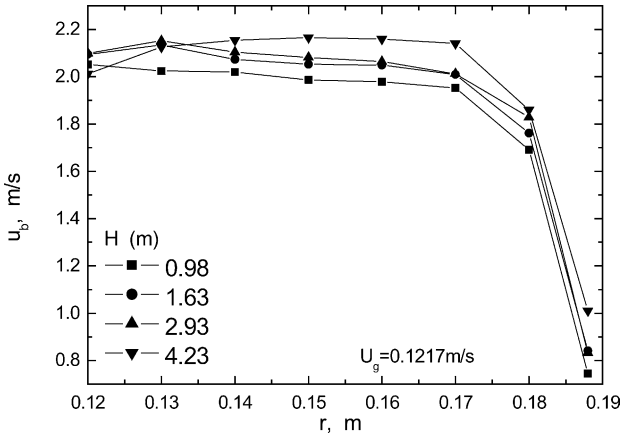


Fig. 3. The axial evolution of bubble rise velocity with increasing axial height.

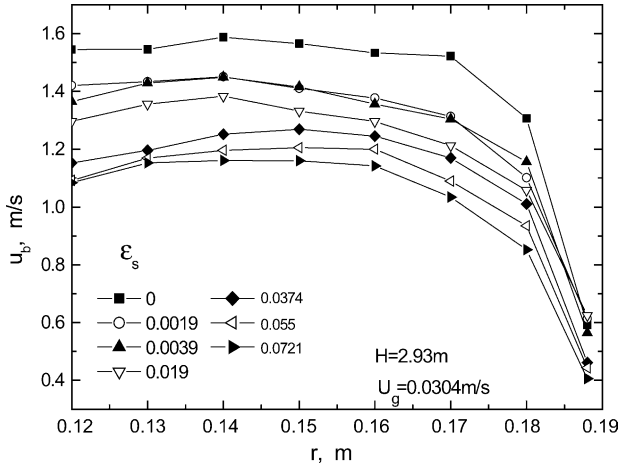


Fig. 4. The effect of solid holdup on the radial profile of bubble rise velocity.

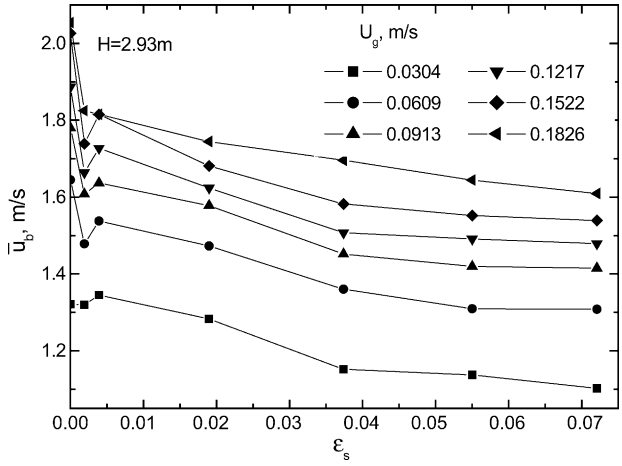


Fig. 5. The effect of solid holdup on the average bubble rise velocity.

bubble rise velocity is more uniform except a steep decrease near the wall of outer tube. A parabolic radial profile appears when the solid holdup is high. This is because with the solid holdup increasing, the wall effect becomes remarkable and the flow resistance near the outer wall of the draught tube increases.

Fig. 5 shows the cross-sectional averaged bubble rise velocity versus increasing superficial gas velocity at different solid holdups. The average bubble rise velocity decreases with increasing solid holdup except that there is an increase in the average bubble rise velocity when the solid holdup increases from $\varepsilon_s = 0.19\%$ to $\varepsilon_s = 0.39\%$. The solid holdup can affect the bubble break and coalescence rates, and higher solid holdup leads to an increase in the flow resistance. Therefore, different effect mechanism will dominate the influence on the bubble rise velocity at different solid holdup. When the solid holdup varies in a range from 0 to 0.19%, the effect of breaking bubble is dominant and an increase in the solid holdup leads to a decrease in the bubble size and the bubble rise velocity [13]. With an increase in the solid loading, the effect of bubble coalescence becomes dominant and the bubble size increases which results in an increase in the bubble rise velocity. With a further increase in the solid holdup ($\varepsilon_s > 0.39\%$), the effect of increasing flow resistance is dominant, and the liquid and bubble rise velocities decrease. It is the complex effect of the solid addition on the flow behavior that leads to a complex behavior of the bubble rise velocity with different solid holdups.

### 3.2. Liquid velocity

The liquid circulation pattern between the riser and down-comer of ALRs is an important characteristic that distinguishes them from other types of gas–liquid contacting devices. The liquid velocity is determined by the balance between two parts: one is the hydrostatic pressure driving force due to the different gas holdups between the riser and the down-comer; and the other is the flow resistance along the loop channel, especially through the separator tubes in the ALR.

The liquid velocities in the annular riser are measured using LDV probe at different superficial gas velocities. The radial profiles of the measured liquid velocities under $\varepsilon_s = 0$ and $\varepsilon_s = 1.94\%$ are shown in Fig. 6(A) and (B), respectively. At different solid holdups, the liquid velocity increases with increasing superficial gas velocity. Similar to the radial profile of the bubble rise velocity, the increment of the liquid velocity decreases with increasing superficial gas velocity and the liquid velocity reaches a maximum value at $U_g = 0.1217$ m/s, at which the bubble rise velocity also reaches its maximum. The flow resistance in an ALR is engendered in four parts, the riser, the down-comer, the separator and the direction change at the top and bottom of the reactor. Addition of solids increases the flow resistance and the energy consumed by the liquid flow, even though the liquid velocity is relatively low. It will be discussed in the modeling section. For a gas–slurry system, it will need a relatively larger superficial gas velocity than for a gas–liquid system to reaches the maximum liquid velocity.

Fig. 7 shows the axial evolution of the radial profile of the liquid velocity at $U_g = 0.0304$ m/s. The radial profile of

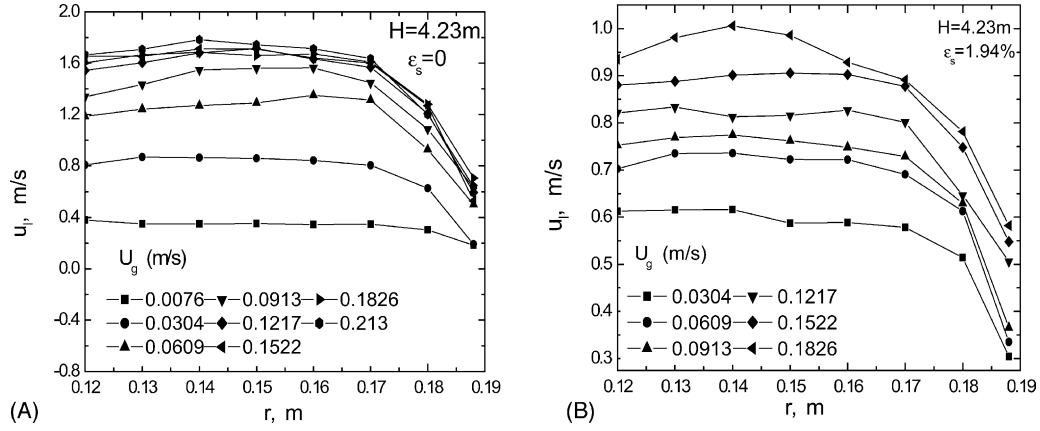


Fig. 6. The radial profile of liquid velocity at different superficial gas velocity.

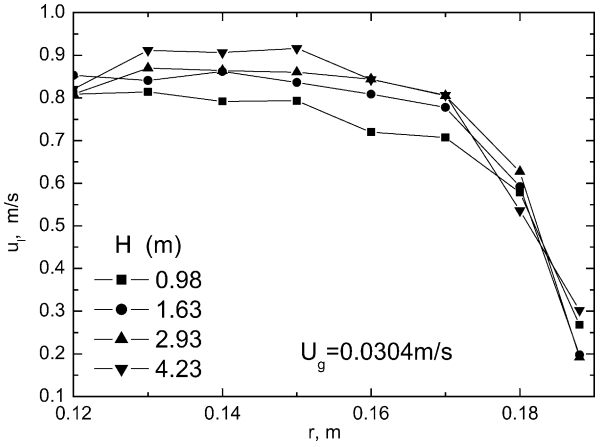


Fig. 7. The axial evolution of radial profile of liquid velocity.

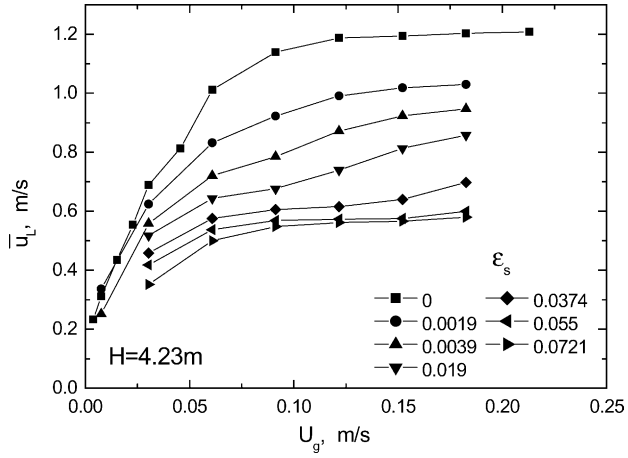


Fig. 9. The effect of solid holdups on the average liquid velocity.

the liquid velocity is flatter at lower positions and become parabolic with increasing axial height. Because of the gas phase expansion along the axial height, the gas holdup increases and the liquid flow channel decreases. So the liquid velocity increases slightly along the reactor axial height.

Figs. 8 and 9 illustrate the radial profile of liquid velocity and the cross-sectional averaged liquid velocity at different solid holdups, respectively. In a liquid–solid system, high solid holdup will increase the superficial viscosity of the slurry and results in an increase in the flow resistance. As shown in Fig. 8, the liquid velocity decreases with increasing solid holdup. Furthermore, the solid holdup also influences the radial profile of the liquid velocity. For the cases of lower solid holdup, the radial profile of the liquid velocity is parabolic. At higher solid holdup, the radial profile is flatter in the inner region. With the addition of solids, the liquid velocity decreases and it tends to give a uniform profile in the radial direction. At different solid holdups, the average liquid velocity increases remarkably with increasing superficial gas velocity firstly. Then it almost keeps constant with increasing superficial gas velocity. Because of the flow resistance increase with increasing solid holdup [14], the energy consumed by the flow increases and the liquid velocity decreases with increasing solid holdup. Klein et al. [15] also found that the liquid velocity decreases with increasing solid holdup.

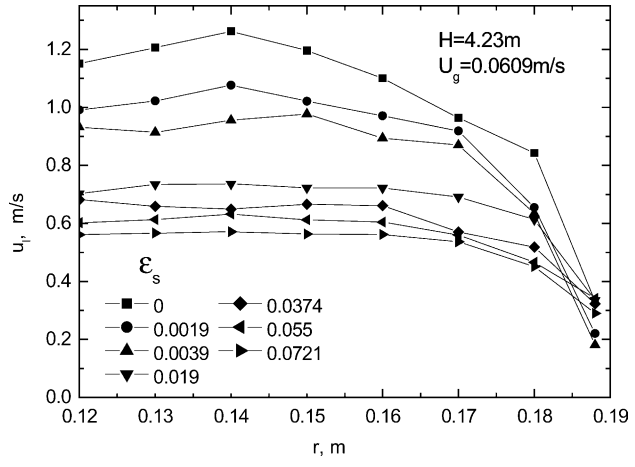


Fig. 8. The effect of solid holdups on the radial profile of liquid velocity.

## 4. Mathematical modeling

Despite a few successful applications, the design and scale-up of ALR still remains in an empirical or semi-empirical stage. One major reason is the lack of reliable mathematical model that can predict the multiphase flow parameters, such as the bubble rise velocity and liquid circulation velocity reasonably. In order to appropriately design and scale-up ALR, a mathematical model is established based on the energy balance model to describe the liquid circulation in the ALR [16]. For the case of the ALR structure used in this work, the model equations of the energy balance is set up by considering the balance between energy input and dissipation in the circulation flow.

The liquid–solid slurry phase was regarded as a pseudo-homogeneous phase with the consideration that the particle size used is very small. Therefore the properties of the slurry phase were calculated from the properties of liquid and the solid holdup. The slurry density can be calculated as:

$$\rho_h = \rho_l(1 - \varepsilon_s) + \rho_s\varepsilon_s \quad (1)$$

The superficial viscosity of the slurry was calculated using following correlation [17]:

$$\frac{\mu_h}{\mu_l} = 1 + \frac{5}{2}\varepsilon_s \quad (2)$$

Two equations are obtained by considering energy balances of the overall reactor and the gas–liquid separator. The bubble rise velocity and liquid velocity can be obtained from these two equations.

### 4.1. Overall energy balance

The overall energy balance consists of inputted energy due to gas expansion $E$, dissipated energy due to flow resistance and turbulence $F$ and the dissipated energy on the gas–liquid interface $S$. That is:

$$E = F + S \tag{3}$$

The inputted energy due to gas expansion in the riser can be determined by:

$$E = P_b U_g \ln\left(1 + \frac{\rho_h g H_r}{P_0}\right) \tag{4}$$

where $P_b$ and $P_0$ are the pressures at the bottom and top of the riser and $U_g$ is the superficial gas velocity at the bottom of the riser.

The dissipated energy due to flow resistance and turbulence $F$ consists of four parts: the energy consumption in the riser, $f_r$, that in the separator tubes, $f_t$, that in the downcomer, $f_d$, and that due to the flow direction changes of the U-bending flow channel at the top and bottom of the reactor, $f_u$. Therefore, $F$ can be written as:

$$F = \sum_i f_i + f_u, \quad i = \text{r, t, d} \tag{5}$$

where

$$f_i = 0.5\alpha\lambda_i\rho_h \frac{H_i}{d_i} u_{l,i}^3 A_i, \quad i = \text{r, t, d} \tag{6}$$

$$f_u = \beta f_r \tag{7}$$

In the above equations, $\alpha$ is a coefficient with the value of 1.0 for single phase flow and 2.0 for multiphase flow [18], and $\beta$ is an adjustable coefficient and has a value of 2.1 by fitting the experimental results for the two phase flow. The flow resistant coefficient is determined by the Blasius equation:

$$\lambda_i = 0.3164\, Re_i^{-0.25} \tag{8}$$

where $Re_i$ is the Reynolds number defined as $Re_i = d_i u_{l,i}\rho_h/\mu_h$ and the diameter of the riser is its hydrodynamic equivalent diameter.

The dissipated energy on the gas–liquid interface $S$ is represented as:

$$S = \varepsilon_g u_{slip}\rho_h g H_r \tag{9}$$

where $u_{slip}$ is the bubble slip velocity and $\varepsilon_g$ the gas holdup in the riser.

Substituting Eqs. (4), (5) and (9) into Eq. (3), the energy balance for the overall reactor reads:

$$P_b U_g \ln\left(1 + \frac{\rho_h g H_r}{P_0}\right) = f_r + f_t\frac{A_t}{A_r} + f_d\frac{A_d}{A_r} + f_u + \varepsilon_g u_{slip}\rho_h g H_r \tag{10}$$

### 4.2. Energy balance in the separator

In order to achieve high efficiency of gas–liquid separation, small diameter of the separator tubes, as shown in Fig. 1, is designed and the velocity of the multiphase stream in the tubes is therefore relatively high. According to the correlation of criterion for slug flow of gas liquid systems given by Das et al. [19]:

$$u_{slug} = 0.35(gd)^{1/2} \tag{11}$$

the minimum velocity for slug flow in the tubes is about 0.2 m/s. This value can be exceeded mostly under all the experimental conditions. Hence it is assume that the flow in the tubes is in slug flow regime. Because air and water flow cocurrently, no relative slip between the phases is assumed which has been observed in experiments. This means that the energy dissipation at the gas–liquid interface, $S$ in Eq. (3), is negligible. Therefore, the energy balance in the separator tube can be written as:

$$P_b U_g \ln\left(1 + \frac{\rho_h g H_t}{P_t}\right) = 0.3164\, Re_t^{-0.25}\frac{H_t}{d_t} u_{l,t}^3 \tag{12}$$

$H_t$, $\varepsilon_{g,t}$, $u_{l,t}$, $P_t$ are the height of the separator tube, the time-averaged gas holdup in the separator tubes, the liquid velocity and the local pressure just above the tube, respectively. Because there is no slip between bubble and liquid, $\varepsilon_{g,t}$ and $u_{l,t}$ can be calculated from the superficial gas velocity, $U_{g,t}$, and superficial liquid velocity, $U_{l,t}$, as:

$$\varepsilon_{g,t} = \frac{U_{l,t}}{u_{l,t}} \tag{13}$$

$$u_{l,t} = U_{l,t} + U_{g,t} \tag{14}$$

The superficial gas velocity in the separator, $U_{g,t}$, can be obtained from the superficial gas velocity in the riser

$$U_{g,t} = U_g\frac{A_r}{A_t} \tag{15}$$

where $A_r$ and $A_t$ are the cross-sectional area of the riser and all the separator tubes.

During the modeling, the bridge effect that addition of solids leads to a decrease in the flow channel has been taken into account. The similar effect was reported by Klein et al. [15]. In order to balance the energy inputted and consumed in the circulation, a modified diameter of the separator tubes is introduced as:

$$d_t = d_t^0(1 - \varepsilon_s)^n \tag{16}$$

The modified diameter is only used to calculate the friction coefficient when solids are added. The exponent $n$ in Eq. (16) can be determined from the experimental data and has a value of 2.0 for this work. Substituting Eqs. (13)–(16) into Eq. (12), the liquid flow velocity in the separation tubes $u_{l,t}$ can be obtained based on the superficial gas velocity and the solid holdup. The superficial liquid velocity in the separator tube, $U_{l,t}$, can be calculated from Eq. (14) if the liquid velocity

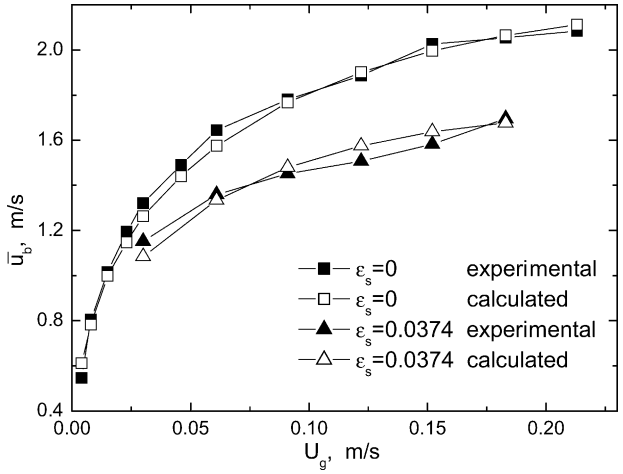


Fig. 10. The calculated and experimental values of bubble rise velocities.

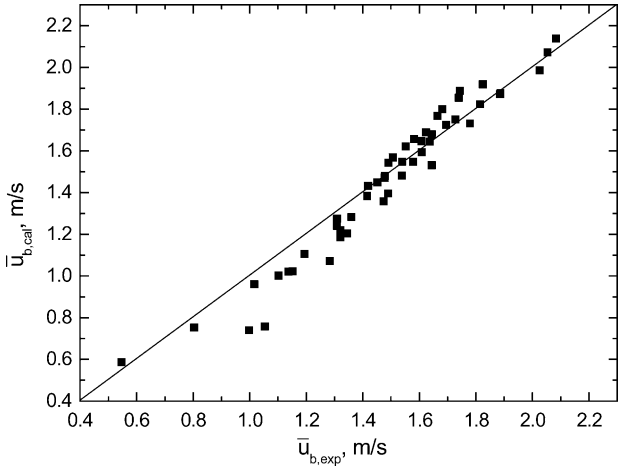


Fig. 12. Comparisons between the calculated and experimental bubble rise velocities.

in the separator tubes is known and the liquid velocity in the riser can be obtained by:

$$u_{l,r} = U_{l,t}\frac{A_t}{A_r(1-\varepsilon_g)} \tag{17}$$

Furthermore, the average bubble rise velocity and the slip velocity in the riser can be calculated the following equations, respectively:

$$u_b = \frac{U_g}{\varepsilon_g} \tag{18}$$

$$u_{slip} = u_b - u_{l,r} \tag{19}$$

### 4.3. Model validation

Based on the mathematical model established above, the hydrodynamic parameters of the multiphase flow in ALRs, such as bubble rise velocity and liquid velocity, can be predicted. The predicted values are compared with the experimental results, as shown in Figs. 10–13. Figs. 10 and 12 show the comparisons of the calculated bubble rise velocity and the cross-sectional average of the measured bubble rise velocities. There is a satisfactory agreement between the measured and calculated results of the bubble rise velocities, for both cases of the gas–liquid system and gas–slurry system.

The comparison results between the measured and calculated values of cross-sectional mean liquid velocities are shown in Figs. 11 and 13. It also shows a relatively satisfactory agreement between the experimental and calculated mean liquid velocities in the operating conditions of this work. Therefore, it is reasonable to conclude that the energy balance model established in this work can describe the circulation flow behavior in the ALR. The experimental measurements supply important basic data for the three-phase reactor development and simulation. And the mathematical model is helpful for the design and scale-up of ALR for gas–liquid and gas–slurry systems.

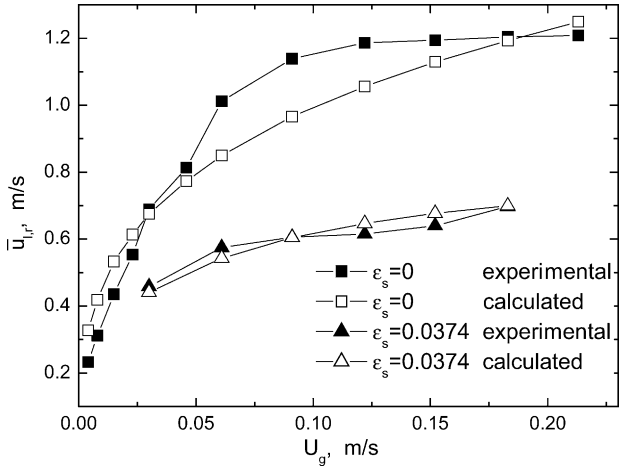


Fig. 11. The calculated and experimental values of the liquid velocities.

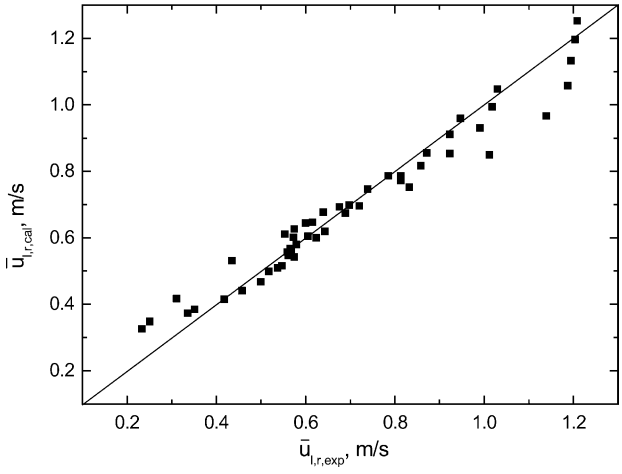


Fig. 13. Comparisons between the calculated and experimental liquid velocities.

## 5. Conclusions

Hydrodynamic behaviors of a novel airlift loop reactor have been studied for cases of gas–liquid and gas–slurry systems under different operating conditions. A novel gas liquid separator with high efficiency has been proposed and an energy balance model has been established for describing the circulation characteristics of the multiphase flow. From the experiments and hydrodynamic modeling we can draw the follow conclusions:

- The bubble rise velocity increases with increasing superficial gas velocity and increases modestly along the axial height due to the pressure decreasing. The solid holdup has influence on the radial profile of bubble rise velocity. At low solid holdups, the radial profile of the bubble rise velocity is uniform, whereas it tends to be parabolic with increasing solid holdup.
- The liquid velocity increases with increasing superficial gas velocity under different solid holdups, but this increase becomes weaker at high superficial gas velocity. The liquid velocity decreases with increasing solid holdup due to the increase of flow resistances and increases slightly with increasing the axial height because of the gas expansion.
- A mathematical model is established based on the energy balance for describing the hydrodynamic behaviors in ALR. The cross-sectional averaged bubble rise velocity and liquid velocity can be calculated from the proposed model. The model can be used for the design and scale-up of ALR of gas–liquid and gas–slurry systems.

## References

[1] C. Vial, S. Poncin, G. Wild, N. Midoux, A simple method for regime identification and flow characterization in bubble columns and airlift reactors, Chem. Eng. Process. 40 (2001) 135–151.
[2] R.S. Oey, R.F. Mudde, L.M. Portela, H.E.A. van den Akker, Simulation of a slurry airlift using a two-fluid model, Chem. Eng. Sci. 56 (2001) 673–681.
[3] K. Koide, M. Kimura, H. Nitta, H. Kawabata, Liquid circulation in bubble column with draught tube, J. Chem. Eng. Jpn. 21 (1988) 393–399.
[4] J. Korpijarvi, P. Oinas, J. Reunanen, Hydrodynamics and mass transfer in an aircraft reactor, Chem. Eng. Sci. 54 (13–14) (1999) 2255–2262.
[5] J. Klein, S. Godo, O. Dolgos, J. Markos, Effect of a gas–liquid separator on the hydrodynamics and circulation flow regimes in internal-loop airlift reactors, J. Chem. Technol. Biotechnol. 76 (2001) 516–524.
[6] K.H. Choi, Y. Chisti, M. Moo-Young, Influence of the gas–liquid separator design on hydrodynamic and mass transfer performance of split-channel airlift reactors, J. Chem. Technol. Biotechnol. 62 (1995) 327–332.
[7] T.F. Wang, J.F. Wang, W.G. Yong, Y. Jin, Bubble behavior in gas–liquid–solid three-phase circulating fluidized beds, Chem. Eng. J. 84 (2001) 397–404.
[8] J. Lin, M.H. Han, T.F. Wang, Experimental study on the local hydrodynamic behavior of a three-phase external loop airlift reactor, Ind. Eng. Chem. Res. 43 (2004) 5432–5437.
[9] C.S. Lo, S.J. Hwang, Local hydrodynamic properties of gas phase in an internal-loop airlift reactor, Chem. Eng. J. 91 (2003) 3–22.
[10] K. Tsuchiya, A. Furumoto, L.S. Fan, J. Zhang, Suspension viscosity and bubble rise velocity in liquid–solid fluidized beds, Chem. Eng. Sci. 52 (1997) 3053–3066.
[11] A.G. Livingston, S.F. Zhang, Hydrodynamic behavior of three-phase (gas–liquid–solid) airlift reactor, Chem. Eng. Sci. 48 (1993) 1641–1654.
[12] J.W.A. De Swart, R.E. Van Vliet, R. Krishna, Size, structure and dynamics of 'large' bubbles in a two-dimensional slurry bubble column, Chem. Eng. Sci. 51 (1996) 4619–4629.
[13] A.S. Khare, J.B. Joshi, Effect of fine particle on gas holdup in three-phase sparged reactors, Chem. Eng. J. 44 (1990) 11–25.
[14] B. Kochbeck, M. Lindert, D.C. Hempel, Hydrodynamics and local parameters in three-phase-flow in airlift-loop reactors of different scale, Chem. Eng. Sci. 47 (1992) 3443–3450.
[15] J. Klein, A.A. Vicente, J.A. Texixeira, Hydrodynamic considerations on optimal design of a three-phase airlift bioreactor with high solids loading, J. Chem. Technol. Biotechnol. 78 (2003) 935–944.
[16] E. Garcia-Calvo, A. Rodriguez, A. Prados, J. Klein, A fluid dynamic model for three-phase airlift reactors, Chem. Eng. Sci. 54 (1999) 2359–2370.
[17] D.Z. Zhang, A. Prosperetti, Momentum and energy equations for disperse two-phase flows and their closure for dilute suspensions, Int. J. Multiphase Flow 23 (1997) 425–453.
[18] M.A. Young, R.G. Carbonell, D.F. Ollis, Airlift bioreactors: analysis of local two-phase hydrodynamics, AIChE J. 37 (1991) 403–428.
[19] G. Das, P.K. Das, N.K. Purohit, A.K. Mitra, Rise velocity of a Taylor bubble through concentric annulus, Chem. Eng. Sci. 53 (1998) 977–993.